



Arecibo ALFA Array Observations in Search of Lunar Meteoroid-Strike EMPs

Saiveena Kesaraju¹ · John D. Mathews¹ · Phil Perillat²

Received: 20 April 2017 / Accepted: 14 May 2019 / Published online: 29 May 2019
© Springer Nature B.V. 2019

Abstract

We present the preliminary results of a search for transient Electromagnetic Pulses (EMP) associated with the impact of meteoroids on the lunar surface as observed with the Arecibo Observatory ALFA (Arecibo L-band Feed Array) system. The ALFA system is a cluster of seven, dual-linear polarization feeds/beams arranged in a hexagonal manner and operated in the protected L-band region centered at 1.41 GHz. We analyzed 8 TB of data totaling nearly 5.5 h of on- and off-moon observations made in February 2016. We demonstrate the observing strategy and time–frequency methods for the detection and removal of the local-radar transient interference signals while identifying potential EMPs. Local out of band radar interference signals are observed as intermodulation artifacts in the protected L-band. Seven transient wideband EMP events with time scales of less than 10 μ s have been detected following the extensive vetting process we describe. *Assuming* that these EMP-like events originate from gram-sized meteoroid strikes and using *very approximate* hypervelocity impact, plasma production theory, and EMP generation theory, we estimate the progenitor impact meteoroid kinetic energy to be approximately 1.8×10^7 J. Assuming that the observed EMPs are the result of 10 g meteoroid impacts, the resultant meteoroid flux is 3×10^{-7} km⁻² h⁻¹ based solely on lunar surface area observed and net observing period. Implications of the observed transient EMP events, measured lunar noise temperature and the comparison with energy estimates derived from the existing lunar impact optical observations are also discussed.

Keywords EMP · Electromagnetic pulse · Arecibo · Moon · Meteoroid flux

1 Introduction

Based on lunar meteoroid impact optical flash observations (Suggs et al. 2008, 2014; Rembold and Ryan 2015), various theoretical hypervelocity impact models (Foschini 1998; Nemtchinov et al. 1998), we hypothesized in an earlier paper, Kesaraju et al. (2016), that

✉ John D. Mathews
JDMathews@psu.edu

¹ Radar Space Sciences Lab, The Pennsylvania State University, 323 Electrical Engineering East, University Park, PA, USA

² Arecibo Observatory, Arecibo, PR, USA

when gram-sized, hypervelocity meteoroids impact the Moon, RF Electromagnetic Pulses (EMPs) are generated in the initial stage of the impact ejecta plasma evolution. Further, based on the laboratory experiments regarding RF emissions due to hypervelocity impacts (Close et al. 2013; Maki et al. 2004, 2005; Collette et al. 2013) it is hypothesized that these EMPs will have a duration of a few microseconds and exhibit a broad frequency extent that includes at least the V/UHF frequency region (30 MHz to 3 GHz) thus setting the stage for the observations, analysis approach, and the preliminary results we report herein.

In 2014, simultaneous UHF (425–445 MHz) radio observations were conducted at Arecibo (AO) and Haystack Observatories to establish the possibility of detecting lunar meteoroid impact EMPs and, thus, to test the above hypothesis. Unfortunately, terrestrial radar signals reflected off the Moon, i.e. terrestrial-origin Moon-bounce (TOMB) signals, dominated our detection scheme. Further, unknown but relatively transient (of the order of few microseconds in duration) and wideband ($\gtrsim 14$ MHz) signals, that are consistent with lunar origin, impact EMPs were observed in two different bands of data collected at Arecibo. However, these signals were not seen at Haystack Observatory possibly due to overwhelming local interference from amateur band repeaters and power-line interference (Kesaraju et al. 2016). Similar detection of transient EMP arc-produced signals that occur due to the contamination of GPS satellite solar arrays was studied at AO as reported by Ferguson et al. (2014, 2016, 2017). While the Ferguson et al. observations at AO were conducted at 327 MHz on-source (GPS satellite) and, for noise and interference reference, off-source at 432 MHz, the interference environment and various processing techniques meant to counter interference effects are very similar to what we report here and in Kesaraju et al. (2016). The Ferguson et al. observations further demonstrate the flexibility and sensitivity of the Arecibo observing system but underscore the difficult interference environment. Having established the viability of the ALFA system for EMP searches within the cold-hydrogen “protected” (1370–1427 MHz; <http://www.setileague.org/articles/protectd.htm>), we used this system to search for the lunar meteoroid strike EMPs as reported below.

The ALFA feed/receiver system consists of a cluster of seven cooled, dual-linear polarization horn feeds (A and B polarizations) arranged in a hexagonal manner as shown in Fig. 1. This system is mounted on a turnstile platform such that it can be rotated into place in the Gregorian optical system above the AO 300 m spherical cap dish. The AO Gregorian optics is comprised of three components; the primary spherical reflector and the secondary and tertiary reflectors inside of the Gregorian dome such that they focus onto the optical plane where the ALFA horn-feed system is located. The HPBW (Half-Power Beam Width) of the individual beams is ~ 3.35 arcminutes with a net elliptical beam pattern (Heiles 2014). In Fig. 1 the beams are represented as circular for simplicity. The full-array edge-to-edge beam width of ~ 14.3 arcminutes (including sidelobes) is useful in searching for impacts on a net larger lunar surface area compared to the ~ 13.2 arcminutes beamwidth coverage of the 440 MHz Gregorian feed that was used in the previous observations. We assume that EMPs occurring anywhere within the net ALFA pattern, including sidelobes, will be potentially detectable. The Moon subtends ~ 30 arcminutes.

A major advantage of the AO ALFA observational setup is that both the dark- and sun-illuminated portions of the Moon can be observed simultaneously unlike the full-dark Moon needed for the most sensitive optical meteoroid “flash” observations. Suggs et al. (2014) describe lunar optical-flash observations, conducted primarily during meteor showers, of 266.88-hours total duration and with an effective lunar surface “collecting” area of 3.8×10^6 km² ($\sim 10\%$ of the lunar surface area). In this observing period, 104 events were detected to a limiting (statistically largest) energy of 1.3×10^7 J (assuming luminous efficiency of 1.29×10^{-3}) yielding a meteoroid flux (flash events over total

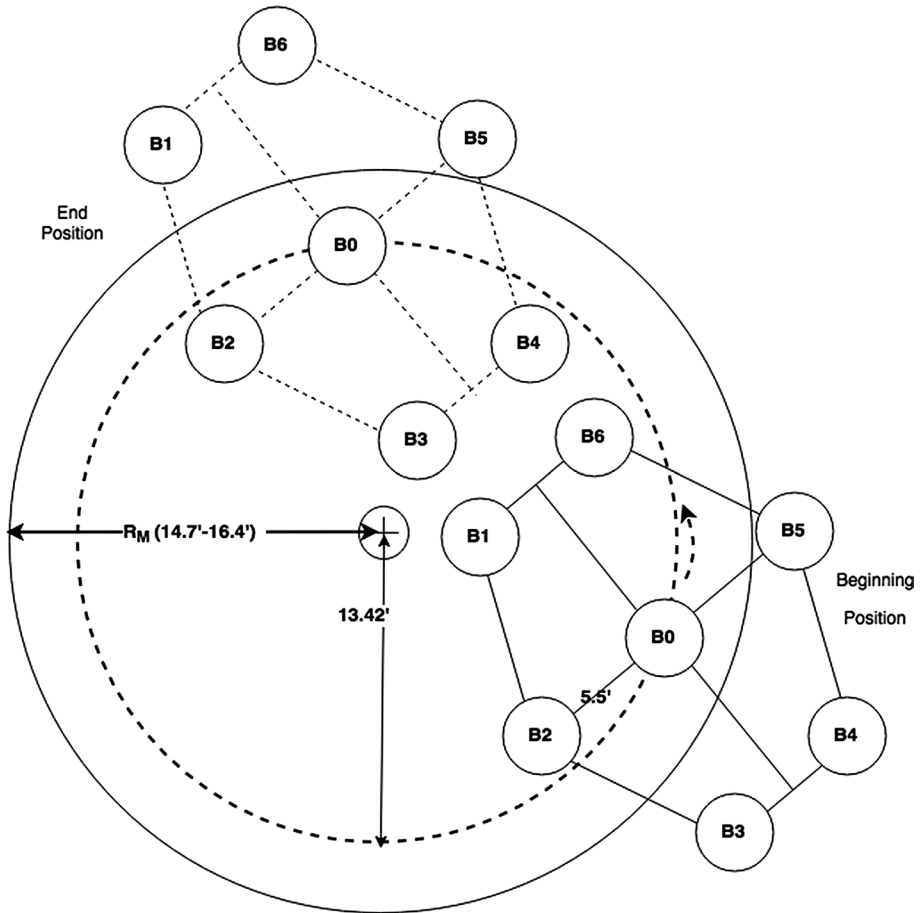


Fig. 1 Illustration of the ALFA beam distribution on the Moon at the beginning (lower right) and end (top left) of tracking. R_M represents the radius of Moon in terms of the angular size (in arcminutes). The dashed circle shows a constant offset of 13.42' from the center point. The 7-beam ALFA system was tracked such that Beam-0 slid along the locus of the dashed circle. In this figure, initially Beams-3,4,5 are pointed off-Moon while Beams-0,1,2,6 are on-Moon. The end-of-tracking positions are shown above center. Note that the beam positions on the sky retain the same orientation but that the illumination-location on the Moon for each beam shifts during tracking

observing period and observed area) of $1.03 \times 10^{-7} \text{ km}^{-2} \text{ h}^{-1}$ for this class of meteoroids. This flux corresponds to ~ 2 optical impact flash events over their net observed surface in 5.5 h. This is slightly lower than the impact flux ($1.09 \times 10^{-7} \text{ km}^{-2} \text{ h}^{-1}$) estimate based on 51 optical-flash impacts detected over 80.97 h duration reported by Rembold and Ryan (2015).

In our case, considering the full ALFA array edge-to-edge beam width (~ 14.35 arcminute) pointing on the Moon that is at $365.8 \times 10^6 \text{ km}$ average distance (assuming sidelobe coverage of the entire area), the lunar surface collecting area is $\sim 7.29 \times 10^6 \text{ km}^2$ ($\sim 19\%$ of the lunar surface area). However, as noted later, only 4 of the 7 beams were continuously “on-moon”. Further, we note that AO observing time is constrained to

when the Moon is transiting near the zenith as the beam pointing extends to only about 20° zenith angle. In addition to the Moon transiting near the zenith, we required the maximum sporadic meteoroid flux to the ALFA-visible lunar surface. As discussed in the next section, no appropriate meteor showers were available. Thus, to maximize ALFA-visible lunar surface exposure to the sporadic meteoroid flux, only the first quarter phase of the Moon is considered as it is only during this phase that a significant fraction of the AO-visible lunar surface faces into the apex-of-Earth's-way and thus to the maximum in sporadic meteoroid flux. This observing geometry is equivalent to the dawn maximum in the meteor rate for mid- and low-latitude Earth-bound observers. This observing geometry is explained in detail in Fig. 1 of Kesaraju et al. (2016). The net observing situation just outlined limits the maximum observing duration to ~ 5.5 h once a month which would result in observing about *four* optical flash impact events (OFIE) based on the flux rate derived from optical observations described above. We *assume* that OFIEs will also coincide with EMPs although we have no a priori way of determining the EMP bandwidth. As the ALFA observational setup is suited for observing both the illuminated and dark sides of the Moon, the number of meteoroid impact events that generate EMPs is expected to be larger than the value derived from the optical flux rate during the meteor shower period. Additionally, as the initial plasma density may increase with decrease in meteoroid mass size due to the smaller penetration depth and volume (Close et al. 2010), we expect to observe the impacts of relatively lower mass (gram-size) than those observed in the optical-flash regime (kilogram-size). Should they prove detectable, the gram-class meteoroid flux should be much larger than the optical-flash-producing meteoroid flux (Ceplecha et al. 1998; Mathews et al. 2001). It may be that the EMP event rate yields the first impactor mass estimates on the way to estimates based on more fundamental physics.

2 Data Collection

As outlined just above, the data collection process was determined by the lunar observation and data-taking constraints of the AO antenna and receiver systems. Appropriate observing geometry with the first-quarter-phase Moon transiting near zenith at Arecibo occurred on the dates given in Table 1. In this observational scenario, the AO-observable lunar face is not directly exposed to any showers. However, the most reliable, high-rate (sporadic) meteoroid source is that related to the apex of Earth's way. A more detailed discussion of this observational scenario is given in Kesaraju et al. (2016). As the observing time does occur during known meteor shower events to Earth (<https://www.amsmeteors.org/2016/02/meteor-activity-outlook-for-February-13-19-2016/>), we note that the following showers are on or below on the lunar subradar point horizon during these observations: α -Centaurids: ZHR ~ 3 peaks 13 Feb extends 2–25 February (southern hemisphere);

Table 1 Observing schedule, Moon phase, and lunar transit time information

Date	Observing period (UT) (within ± 20 degrees of zenith)	Moon phase	Transit time (UT)	Maximum elevation of the moon at transit (degrees)
14 Feb 2016	20:45 to 23:30	0.46	22:09	85
15 Feb 2016	21:45 to 00:25	0.57	23:00	87.5

θ -Centaurids: ZHR~4 peaks 14 February extends 23 January–12 March (southern hemisphere); δ -Leonids: ZHR~2 peak 25 February extends 15 February–10 March; π -Virginids: ZHR~4 peak early March extends 13 February–8 April; δ -Cancrids are concluding. Again, we expect the (small) meteoroid flux from the above meteor shower events at the edges of the lunar surface relative to the sub-radar point.

The apparent size of the source (Moon), also defined as the angular diameter size from the given observing point, is defined as follows

$$\theta = 206265 \frac{d}{D} (\text{arcseconds}) \quad (1)$$

where d is the diameter of the Moon and D is the distance to the Moon as observed at AO. This value can vary between $\sim 29.4'$ and $32.89'$ as the distance to Moon varies between its perigee (363,104 km) and apogee values (405,696 km). During this observation period, the mean angular radius was $\sim 16.3'$. In this observing scenario, the ALFA center beam is tracked and pointed at a total offset of $\sim 13.5'$ from the center of the Moon during the whole observation period. The pictorial representation of this scenario is shown in Fig. 1. The additional offsets to the outer beams of $\sim 5.5'$ results in few beams pointing on-source and few beams off-source at any given time. Beams that are pointed on- and off-source vary continuously as the center Beam-0 “slides” along the locus of the lunar offset center point. Additionally, the rotation angle of ALFA was fixed at zero. That is, the mechanical orientation of the horn feeds on the array is fixed resulting in rotation of the offset beams on the sky as the center beam tracks the moon.

The apparent (pointing coordinates calculated for observing date ephemeris) and J2000 Right Ascension (RA) and Declination (Dec) positions of the center point of the Moon obtained from NASA Horizons Online Ephemeris service were used to point the center beam-0 at an offset and predict the remaining beam positions during the observation periods. Prediction of the total offset of the beam positions with respect to the actual center point of Moon during the observation time on the first day of observations is shown in Fig. 2. As the angular radius of Moon was $\sim 16.3'$ during the observing period (Eq. 1), all of the beam positions in Fig. 2 above $16.3'$ will be pointing off-moon except for possible sidelobe effects. This observational setup of simultaneously observing on- and off-source is useful in identifying and, to some extent, eliminating local interference if present. This beam positioning was most useful and, although we would like to take credit, was the happy accident resulting from inadvertently entering the wrong Julian date for the ephemeris into the tracking program.

Furthermore, the Mock spectrometer receiver system (<http://www.naic.edu/~astro/mock.shtml>) was operated in time domain mode to collect the data from all the 7 dual polarization beams (Beam 3B was not working). The polarization isolation is greater than 20 dB and the center-beam (0) has a somewhat higher gain than the peripheral ones. The low-noise amplifier (LNA) at the front end of the RF receiver of Beam 3B was off during the observation time. The backend of the Mock spectrometer receiver was setup with the first local oscillator frequency centered at 1745 MHz and the first intermediate frequency centered at 335 MHz such that the center of the received bandpass was 1410 MHz. The IF bandpass was complex mixed down to DC and 12-bit sampled at 6.4 MHz. The data thus recorded was stored in the standard Arecibo pdev file format.

To confirm the possible source(s) of the radio frequency interference (RFI) signals described below, we conducted separate off-Moon observations on 21 February 2017. A receiver configuration identical (center frequency and bandwidth) to that before was used

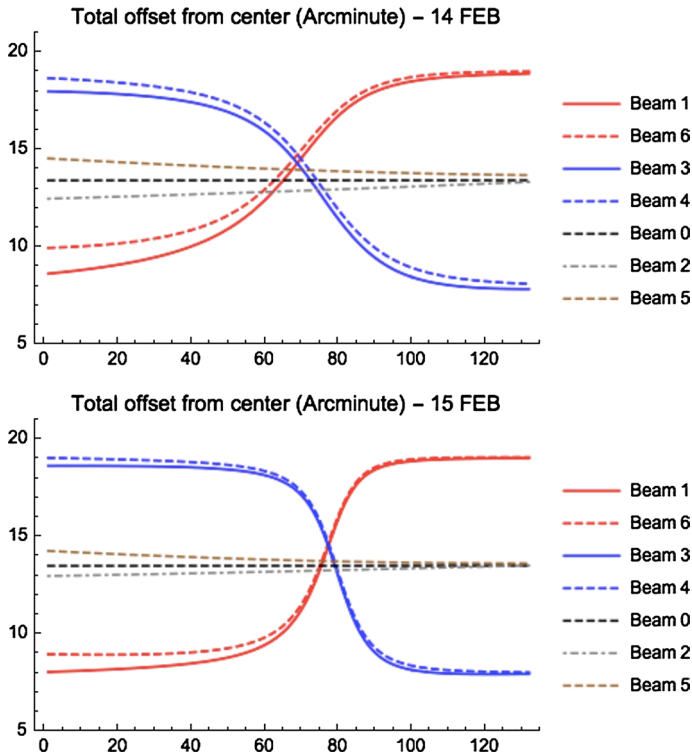


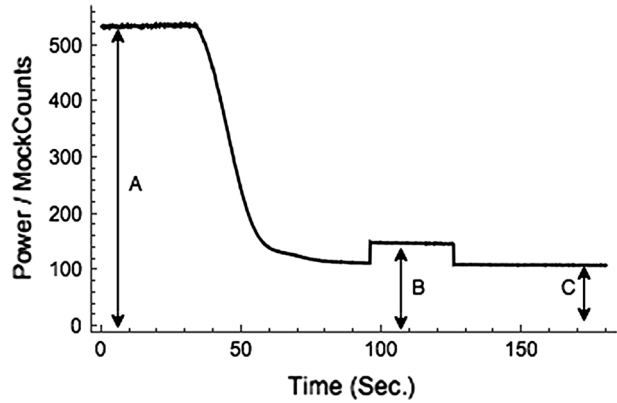
Fig. 2 Total offset of the beam-center positions of the ALFA receiver with respect to the lunar center point at each observing time on each day of observations. This plot is derived from the apparent and J2000 Right Ascension (RA) and Declination (Dec) positions of the center point of the Moon obtained from NASA Horizons online Ephemeris service. The beam positions above 16.3' represent off-Moon pointing directions for the respective beam centers. Note that Beam-5 is pointing at the edge of the Moon

in this case. During these observations, Beam-0A was not functioning due to difficulties similar Beam-3B in the previous observations. The position of the receiver (Gregorian Dome) was varied within 275° to 455° feed azimuth angle at the constant zenith angle of 15° and at a constant azimuth rotation rate of $0.1^\circ/\text{s}$ in both the clockwise and anticlockwise direction in the first and second passes, respectively. One more data collection series was performed at a zenith angle of 10° . The azimuth range was chosen to match the tracking range used in the previous observations. With this setup, the RFI characteristics with respect to the azimuth position were studied. Nearly 1.5 h of this off-Moon data was collected in this mode.

3 Data Processing

In the first pass signal processing, noise temperature at the 1410 MHz center frequency is derived for each receiver. As the Moon thermally radiates (and reflects sky noise) in the microwave region, noise temperature increased, relative to (near lunar limb) sky temperature, as the individual ALFA beams were pointed on-Moon. To calibrate absolute noise

Fig. 3 Increase in noise power due to the induced cal deflection value (B, C). We can also observe the decrease in noise temperature as the Moon drifts out of the beam—levels A transitioning to C. Level C, receiver plus sky noise temperature in Kelvins, is taken to be the system temperature for each receiver



level, a known calibration noise source (cal) is introduced at the beginning and end of the observations. As an example, Fig. 3 shows the introduced cal deflection at the end of the tracking observations (i.e., lunar zenith angle > 20°) observed in Beam 0. The noise value of the off-Moon data (C), the known induced cal deflection (B), and the noise count when the beam is pointed towards the lunar surface (A) are used to determine the approximate lunar temperature during tracking for each beam at both polarizations. The known cal temperatures listed in Table 2 are introduced resulting in noise level increase from C to B. The induced cal deflection counts (B, C) are estimated to determine the temperature (Kelvins) per the Mock-count (W) as in Eqs. 2, 3. Finally, system temperature (the local, near-Moon, sky temperature) is computed as (W×C) which is given in Table 3 for all the beams and both polarizations. As shown in Table 3, the average receiver system temperature (Tsys(K)) is ~33.5 K except in Beam 3. This confirms that Beam3B was not working or was off-source during the observations.

$$T_{cal}(counts) = B - C \tag{2}$$

$$W = \frac{T_{cal}(K)}{T_{cal}(counts)} \tag{3}$$

Table 2 Cal temperatures in Kelvins of each receiver at 1410 MHz

	Beam 0	Beam 1	Beam 2	Beam 3	Beam 4	Beam 5	Beam 6
Pol A	11.76	10.75	11.73	11.29	11.05	11.14	11.67
Pol B	11.07	11.42	11.21	10.59	10.81	9.58	11.29

Table 3 Receiver system temperatures (Kelvins)

Estimated Tsys(K)	Beam 0	Beam 1	Beam 2	Beam 3	Beam 4	Beam 5	Beam 6
PolA	34.49	32.44	36.70	65.77	37.71	32.65	32.80
PolB	34.76	35.46	38.30	565.15	34.37	27.64	31.76

These temperatures include the local sky background contribution per Fig. 3. Beam 3, PolB was off with noise leakage to PolA

In the second pass signal processing, which was designed to detect the transient EMP signals in the data, the crest factor (Peak-to-Average power ratio) is estimated. As the hypothesized EMP event timescale is $\sim 1\text{--}10\ \mu\text{s}$ a processing time window of 100 ms was chosen to determine the average power ratio and to reduce the processing time of the $\sim 5.5\ \text{h}$ of data collected. Peaks that are above a defined threshold (crest factor 12.5 dB), i.e. events that are statistically greater than $\sim 4\sigma$ in either of the polarizations from all the beams, are identified. The formula for computing the crest factor is given in Eq. (4). For a signal with zero mean and a Gaussian distribution, the root-mean-square voltage value is equal to standard deviation and hence the crest factor of 12.5 dB is approximately equivalent to $\sim 4\sigma$. The distribution of the number of peaks detected from all the seven beams and two polarizations with respect to the crest factor are shown in Fig. 4.

$$CF = 20 \log_{10} \frac{V_{peak}}{V_{rms}} \quad (4)$$

4 Results

The on-Moon noise temperature derived from the noise level after subtracting the off-moon noise level (C) in all the 7 beams is shown in Figs. 5 and 6 for both linear polarizations, respectively, on the first and second day of observations. The lunar noise temperature is estimated to be $W \times (A - C)$ for each beam and polarization as the moon is tracked. The near-zero noise temperature observed at the end of the observational data in both polarizations of Beams 1 and 6 confirm that these beams were pointed off-Moon and are in accordance with the predicted beam positions (see Fig. 2). Similarly, at the onset of observations, Beams-3, 4, and 5 were pointed off-Moon. However, Beams 0 and 2 were on-source throughout most of the observational time giving an approximated lunar temperature of $\sim 150\ \text{K}$ at 1.41 GHz.

Similar lunar noise temperature results were also observed at S-Band, X-Band, Ka-Band by Morabito (2006). Further, as mentioned above, real temperature variations at the edge of the Moon (near-limb–large, relative to surface aspect angle) were observed during the onset time in both beam-5 polarizations. Since most of the thermal emission at L-band

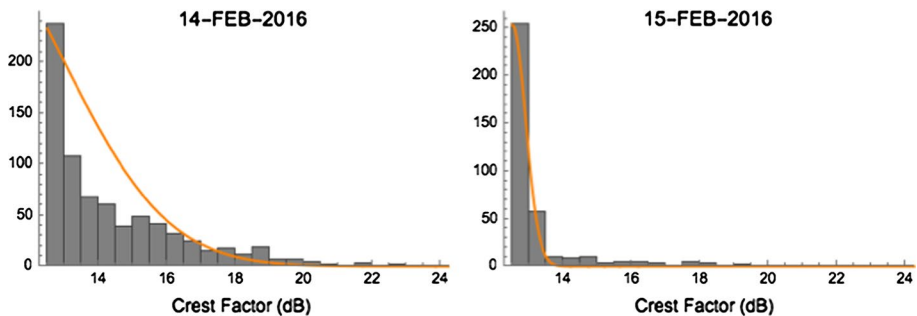


Fig. 4 Distribution of number of peaks detected versus Crest factor (dB; see Eq. 4) greater than 12.5 dB ($> 4\sigma$) from the data collected on 14 Feb 2016 (Left) and respective data collected on 15 Feb 2016 (Right). The difference in distribution on both days is likely due to the strong local PB radar interference on first day. Further vetting for possible EMP events is described in the text

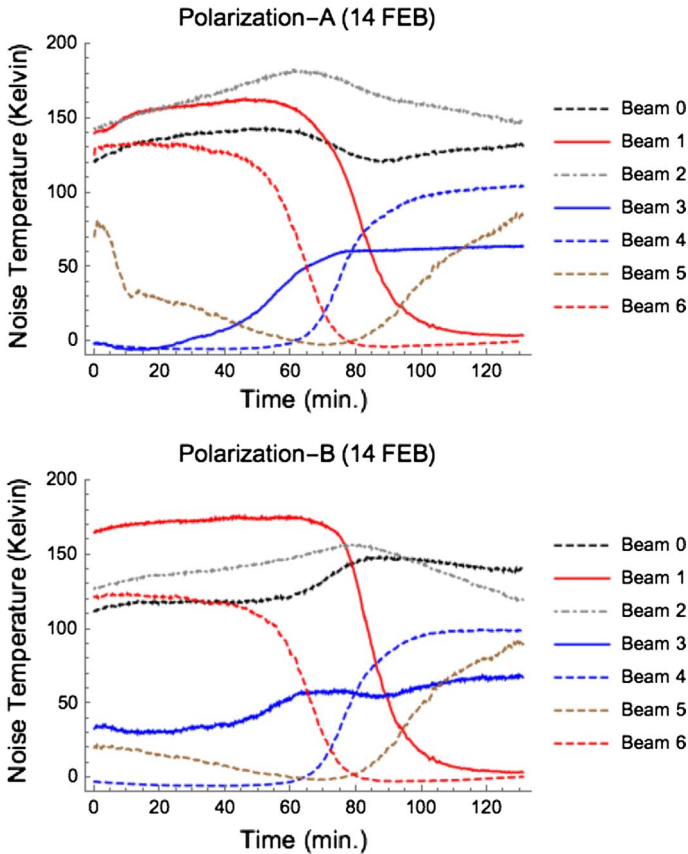


Fig. 5 Net observed noise temperature derived from the measured total noise level after the subtraction of off-moon temperature in Polarizations A and B during the day-one observation period. Noise temperature near 0 K is thus characteristic of beams that are pointed off-Moon as the system plus sky temperature has been subtracted. Curious but real variations at the edge of the Moon were observed during the onset time in the beam-5 polarizations. Also note the opposite-phase features in Beam-0 Polarizations A/B. These features are real and, while appearing to be associated with crossing the day/night terminator, are considered to be a combination of near-limb parallel/perpendicular transmission/reflection coefficients and observing bias introduced by the Fig. 1 beam configuration as described in the text. Note that the polarization features, while very interesting, do not impact the EMP search and will be the subject of future work

originates in the subsurface, at high emission angles (i.e., near/at the limb) the emission is significantly linearly polarized due to the different reflection/transmission coefficients parallel and perpendicular to the plane of emission of sky noise and of subsurface thermal emission (Heiles and Drake 1963; White and Cogdell 1973). The plane of emission is aligned with the radius vector from the center of the Moon and so rotates around the limb. This polarization effect further explains the opposite-phase features in Beam-0 Polarizations A/B. In these observations, we also observed an apparent noise temperature difference between the lunar “day” and “night” sides. Note that similar distinct day-night change in the thermal emission at Ka band, a small effect at X-band, and none at S-band, all using circular polarization, were reported in Morabito (2006). These features are real and, while they appear to be associated with crossing the day/night terminator, are likely artifacts of the polarization effects just described combined with the bias introduced by our observing

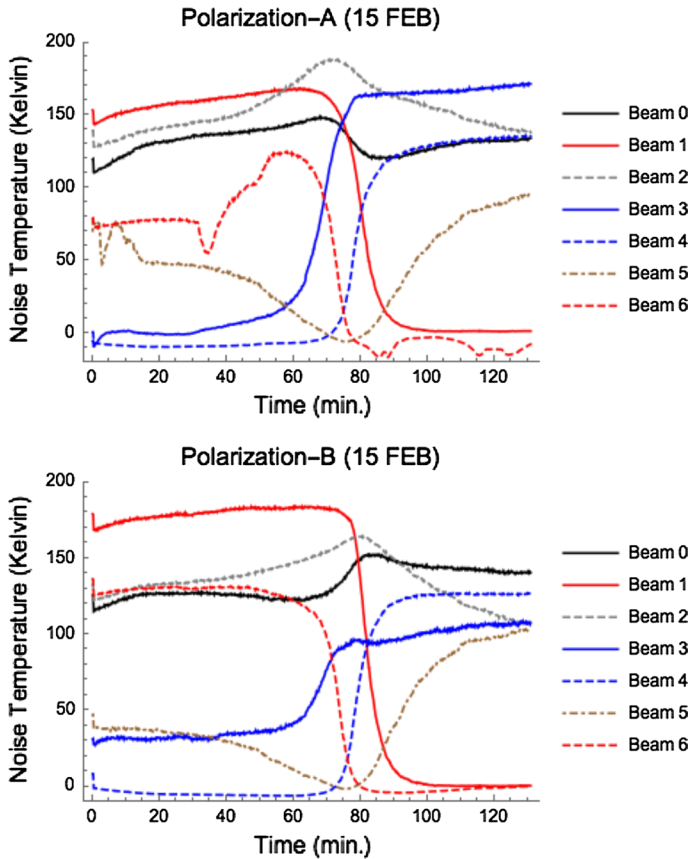


Fig. 6 Similar to Fig. 5, the second-day noise temperature derived from the measured noise level after the subtraction of the off-moon temperature in Polarizations A and B. The initial temperature “glitches” are due to onset of tracking after the moon entered the beam. Again, note the beam0 polarization A/B opposite-phase feature at terminator crossing. See Fig. 5 and text discussion of this feature

mode (see Fig. 1). At this point, this interesting result will be the subject of future work and does not effect our EMP search results. *However, these near-limb polarization effects are likely important to near-limb impact-EMP events.*

To search for candidate EMPs, spectrograms of the detected peak-events were manually analyzed to identify spurious signals. Unanticipated intermods/mixermods or harmonics of the Punta Borinquen (PB) radar (an aerostat radar located to the North-West of AO at frequency 1274.6 MHz) are observed at 1408 MHz (Ellingson and Hampson 2003; Quintero and Perillat 2016) as chirp signals that have a bandwidth of 1.5 MHz. One such event is shown in Fig. 7. These peaks are observed at the end of observations when Beams 1 and 6 are pointed off-source. These are not the Terrestrial Origin Moon Bounce (TOMB) signals which exhibit lunar limb scattering as observed in the previous set of observations at a 435 MHz center frequency (Kesaraju et al. 2016). A priori information available about the PB radar was considered towards understanding this source of interference in the data (<http://www.naic.edu/~phil/rfi/rdr/puntaBorinquen/puntaBorRdr.html>). In particular, the PB radar signal has an inter-pulse period sequence (2–4 ms duration) and exhibits a 12 s

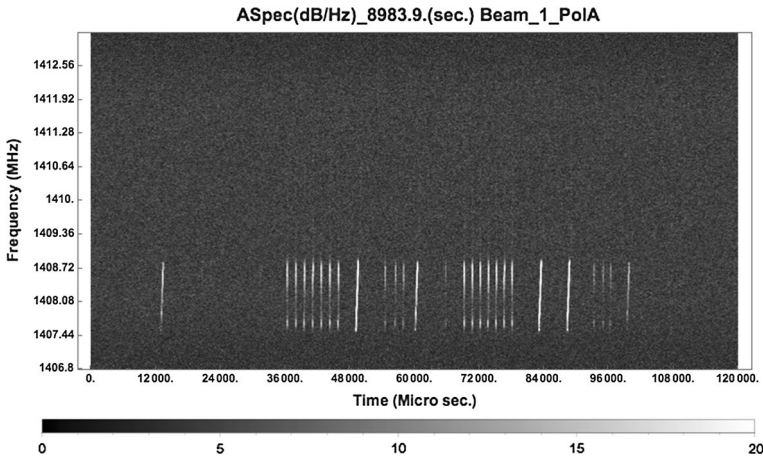


Fig. 7 Spectrogram of Punta Borinquen (PB) radar chirp signal observed in the Beam-1, Polarization-A while this beam was pointed off-Moon. These interference signals are an intermodulation feature generated in the receiver LNAs by the strong out-of-band PB radar signal as its beam sweeps past AO

rotation period modulation. In addition, there is an extended sidelobe-signal of -6.7 dB strength (relative to the main-lobe) within the first 5 s of the rotation period. As a consequence, we observed strong wideband transient peaks (duration of 100–800 μ s) above the crest factor threshold (12.5 dB) in the off-source beams as shown in Fig. 8 (Beams 4 and 5 in first 60 min of observation see Fig. 5) that likely originate with the sidelobe passage interference from the PB radar.

As a further test of our approach, the off-Moon data was also searched for the peaks greater than the 12.5 dB crest factor threshold. Strong transient wideband peaks like that of Fig. 8 were observed. Figure 9 shows the spectrogram of one of such event detected in the off-Moon data. Figure 10 shows the histogram of the number of peaks above the crest factor threshold versus the azimuth angle, which were detected in all the beams (except Beam 0A that was off). Not all of these peaks have a strong wideband nature as shown in the Fig. 9. As shown in Fig. 10, the largest numbers of peaks were observed over 20° – 30° azimuth range angle from the plot start position (feed azimuth angle 275°). The PB radar is located at $\sim 12^{\circ}$ on the Fig. 10 plot.

Additionally, no chirp signals were detected in our search band (~ 1408 MHz) nevertheless we found a few peaks in the time domain as shown in Fig. 11b that show the IPP characteristics of PB radar signal. For comparison, a time series plot of Fig. 7 is shown in Fig. 11a. As the PB radar-RFI signals do not directly illuminate the feed it is possible that the somewhat lower SNR is the cause of not observing the chirp characteristics. Lastly, in the noise data observations, we also observed ~ 14 highly transient peaks in Beam-0A that were also observed in all the remaining beams and polarizations as shown in Fig. 12. As these peaks were observed in the receiver whose low noise amplifier was off, we attribute these peaks to a common internal source such as power-line and/or power supply interference generated near to or within the ALFA receiver system.

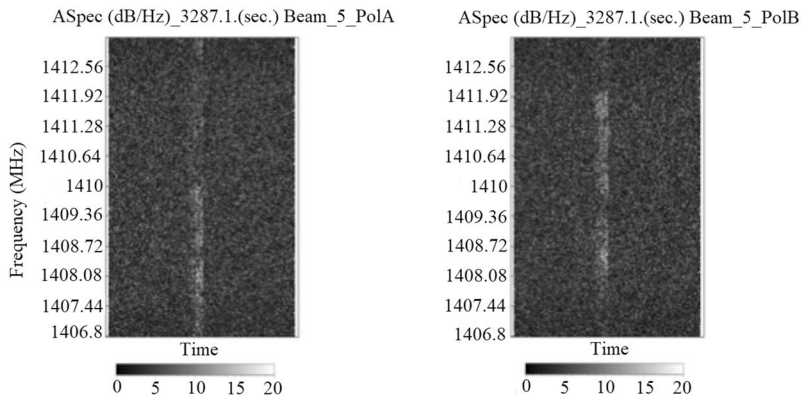
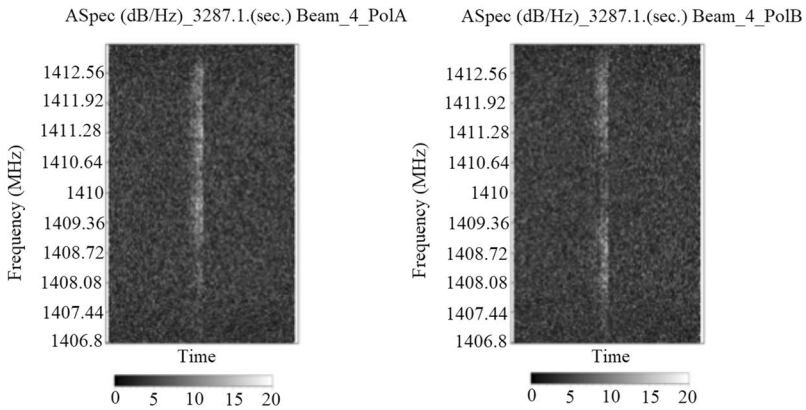
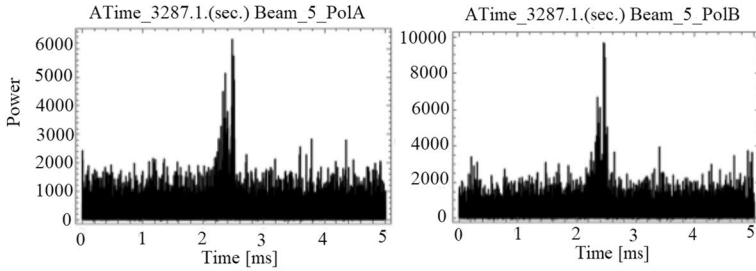
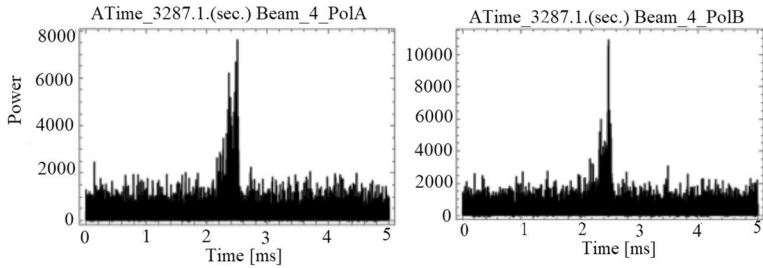
Given the properties of the PB radar intermodulation interference, a mask was generated based on the rotation period (12 s) and the start time of the detected chirp events. Events that occur in RF-interference-free time interval—defined as the interval between 7 and 11 s of the PB radar beam rotation period with respect to the start time of chirp

Fig. 8 Time series and spectrograms of the transient EMP-like interference pulses in both polarizations A and B observed in off-source Beams 4,5 at approximately 54 min from the observation start time on 02–14–2016 observation date (for beam configuration at that time, refer to Fig. 5). These are likely generated from the extended side lobe of the PB radar signal and can be easily identified and excluded

events—were retained for further analysis. Peaks that were observed in only the on-source beams—i.e., Beams-0,1,2,6 in approximately first hour of observations (see Fig. 5) and Beams-0,2,4,5 in the second hour of observations—and were observed in both polarizations, were classified as the hypothesized EMP event signals possibly due to meteoroid strike events on the lunar surface. Further signal discrimination is performed by searching for possible simultaneous but lower-level peaks in other beams (excluding Beam 3B which was off during the observations). *In particular, a seemingly correlated signal in an off-Moon beam rejects the event.*

To illustrate the next analysis steps, we use a candidate-EMP event, event no. 3 in Table 5 (see Fig. 13), that was initially identified in Beam 6, PolA, as an example to estimate the impact velocity from the observed event RF energy. This event was observed at ~20:50 UTC on 14 Feb 2016 (approximately 2661.6 s or 44.3 min from the start time). The width of the PolA signal is 1.5 μ s. The background noise is subtracted and the received power flux density of this signal, using a 225 m illuminated-dish radius and 6.4 MHz bandwidth, is estimated to be 10^{-11} W/m²/Hz. Assuming the distance to Moon from the observing location to be 384,400 km and that the signal radiated uniformly into a half-sphere, the power spectral density of this signal is calculated to be in the range of 3.7–7 W/Hz in both of the polarizations of Beam 6. Note that the individual polarization features are somewhat offset in time, a fact, that if this is an impact EMP, is important to the physics of the process. The net conversion efficiency (η) of impactor meteoroid kinetic energy to plasma creation and the resultant RF emission is assumed to be in the range of 10^{-4} – 10^{-2} %. This is estimated on the basis that the immediate temperature of the plasma produced is in the range of 20–40 eV (Ratcliff et al. 1997; Close et al. 2010) with initial peak plasma number density in the range of 10^{16} – 10^{18} m⁻³ (Close et al. 2004) and assuming a meteoroid mass in the range of 1–30 gm with impact speeds in the 11–72 km/s hypervelocity range. As noted earlier, for a given event, a decrease in assumed meteoroid mass implies an increase in the conversion efficiency (η). Table 4 shows some possible velocity results and mass estimates (i.e., event KE) for different efficiency rates for this event considering the RF emission across the receiver bandwidth of 6.4 MHz. Again, we do not know details of EMP generation, nor do we know impactor parameters. *The point of these observations is to begin to understand the processes involved in a regime that is otherwise not accessible.*

Over the ~5.5 h observing period in the on-Moon beams, a total of seven possible impact EMP events were identified. Details of these events are given in Table 5. Note that the PB radar blanking and interference characteristics were same on both days although, as shown in Fig. 4, the crest-factor statistics were different. The non-uniformity in the number of events detected on each day can possibly be attributed to difference in the “phase” of the Moon relative to the apex of Earth’s way or, more likely, simply statistical fluctuation. More observations are needed to sort this out. Further, not all of these possible events were present in both polarizations at the same time (except Event No. 5). As we do not understand the physics of EMP generation in this situation, especially given the dielectric properties of the lunar surface material, this is an important result IF these are indeed impact EMPs. Figures 13 and 14 shows the dual polarization results of the remaining possible events detected and Table 5 shows the respective crest factor thresholds and the estimated



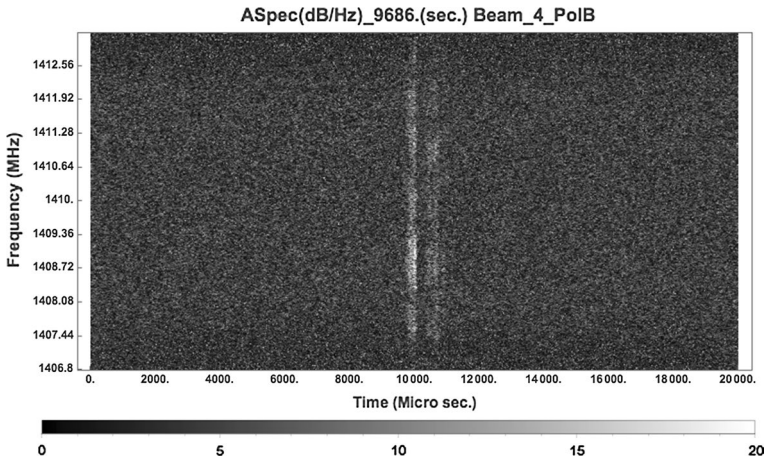


Fig. 9 Spectrogram of one of the transient wideband RFI event observed in the separate off-Moon data collected on 02–21–2017. The broadband spectrogram shows the full effects (at ~ 1408.5 MHz) of the inter-modulation signal due to the out-of-band PB radar interference. Similar signals were also generated via an extended side lobe of the PB radar signal during the on-Moon ALFA observation dates as shown in Fig. 8

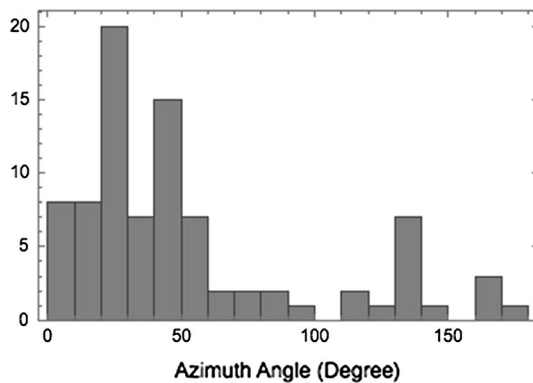


Fig. 10 Histogram of number of peaks versus azimuth angle, starting from feed azimuth angle of 275° , as detected in all the seven beams of ALFA from the separate off-Moon observations collected on 02–21–2017. These peaks are at or above the crest factor threshold (12.5 dB) excluding Beam-0 (which was off). The PB (Punta Borinquen) radar azimuth angle is $\sim 287^\circ$ (12° above) with respect to AO. The largest number of peaks were observed over 20° – 30° (295° – 305° total azimuth angle)

kinetic energy. *These potential events have been very conservatively chosen although no five-sigma events were found.*

Unfortunately, no simultaneous optical observations of the Moon were available for the observing periods reported herein. Also, in all of our results, we cannot totally rule out noise impulses from unknown local interference sources. However, we consider the Table 5 events to *likely* be lunar-meteoroid strike EMPs. The (limiting) kinetic energy (herein, the approximate highest detected kinetic energy) estimate value is 1.8×10^7 J and we *assume* $m = 10$ g and efficiency value of 0.001%. The mass and KE conversion efficiency (η) are chosen based on the Table 4 considerations. Note that, while there is large

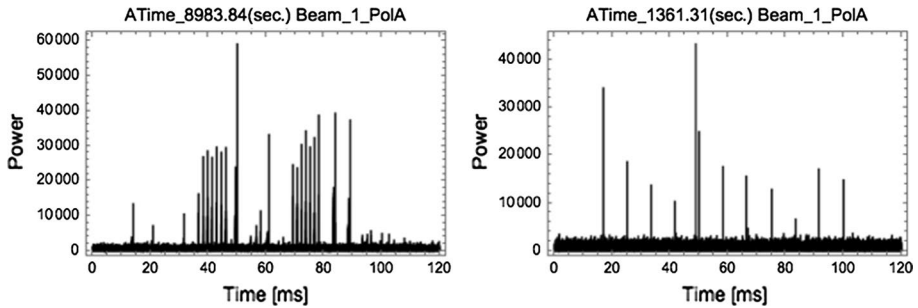
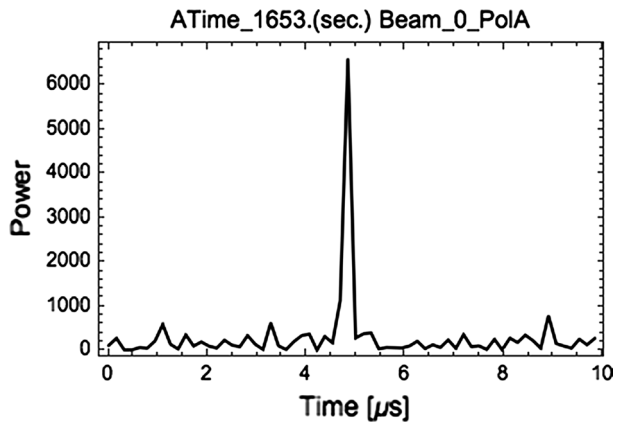


Fig. 11 Left: Time series plot of the RFI event observed in 2016 dataset and shown in Fig. 7. Right: Time series plot of a similar RFI event observed in the 2017 off-Moon dataset. This signal displays periodicity (in the range of 5–15 ms) and can thus be attributed to local RFI. These peaks were also observed in all the remaining beams and polarizations (except Beam-0A that was off) and thus easily identified as RFI

Fig. 12 A transient peak observed in the off-Moon 2017 dataset in the Beam-0A receiver for which the low noise amplifier (LNA) was off during the observations. This peak was also observed in all the remaining six beams and in both polarizations thus enabling easy identification. These features were possibly generated in the power supply chain within the ALFA receiver



uncertainty in meteoroid mass and cumulative number flux to Earth, the whole-earth number of 10 grams and larger events annually is taken to be about 23 times larger than 1 kg and smaller events [Fig. 25, Table 25, Ceplecha et al. (1998); discussion surrounding Fig. 2, Mathews et al. (2001)]. These results are similar to the limiting kinetic energy estimate value of $\sim 1.05 \times 10^7$ J derived from lunar impact optical flash observations of 126 events as described in Suggs et al. (2014). However, given our limited observing time and effective observing area, plus all of the other unknowns, we choose 10 gm and larger impacting meteoroids to *illustrate the possibilities*. Note that the apparent impactor kinetic energy of the Fig. 7 interference signal, if it was attributed to an impact, is $\sim 3.06 \times 10^7$ J. This is greater than the limiting kinetic energy estimate value of the Table 5 proposed impact events and points to the difficulty in sorting through the observed data.

5 Discussion

We report on passive radio observations of the Moon that were conducted using the Arecibo Observatory 7-beam ALFA feed/receiver system to search for ElectroMagnetic Pulses (EMPs) generated by meteoroid strikes on the lunar surface. Our expectations were (and

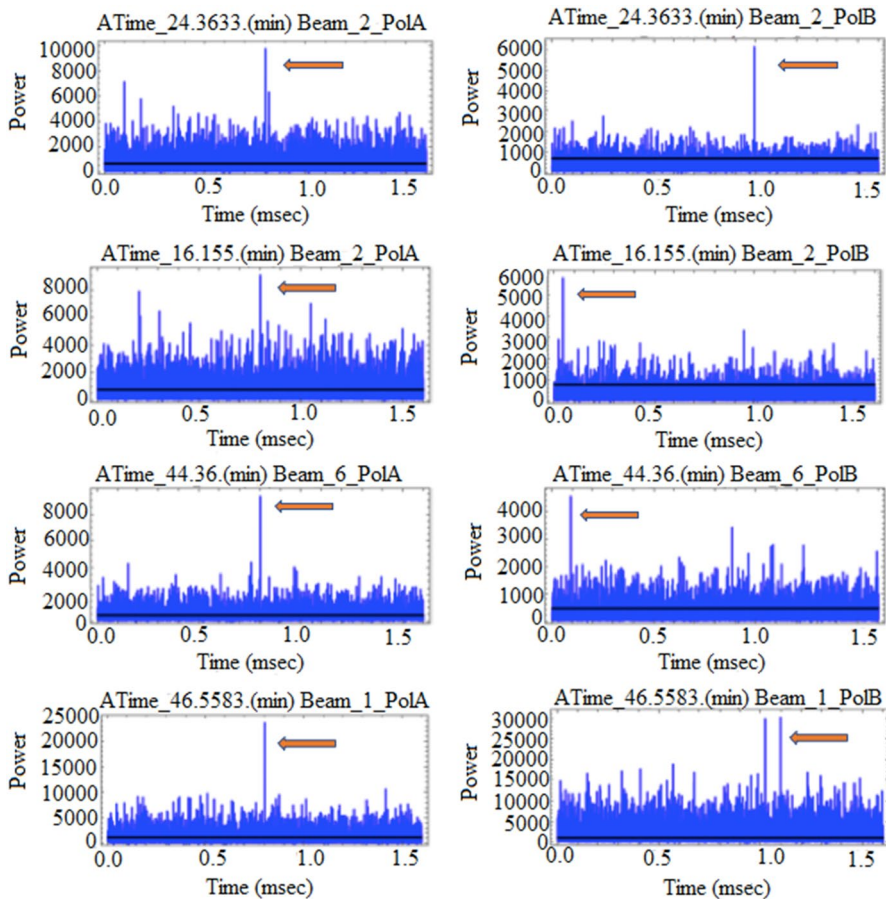


Fig. 13 Power versus time plots for Events 1–4 in both polarizations of the seven possible transient EMP events observed in the respective beams. Each row shows the “finalist” event observed in the respective beam in a 1.6 ms window. Events in the left column are observed in Polarization A and to the right side are observed in Polarization of B. The black lines indicate the average power calculated from the sliding 100 ms time window

remain) that lunar meteoroid strikes generate broadband EMPs. However, the impact physics, ensuing plasma physics, and radio science of EMP generation are not well understood. We, in part, undertook these observations to better understand the impact/EMP physics. In particular, given the sensitivity of the ALFA system, only a very small fraction of meteoroid kinetic energy needs to be converted to a broadband EMP for AO detection. But other than for the microsecond time scales corresponding to the actual impact, we know little about the properties of the EMP generated by gram-sized meteoroids traveling at the expected speeds. But the open question is that, if EMPs are not observed (and meteoroid-strike optical flashes are), why? For example, while we expect EMPs to be observed (nearly) simultaneously in both polarizations, that is an assumption. We report detection of seven, highly-vetted “finalist” EMP-like impact events. Our signal processing and vetting approach are of community interest and have been discussed in detail on the way to presenting the seven “finalist” events.

Table 4 A range of impactor velocity estimates yielding the energy detected in event 3 (Event no. 3 in Table 5) as a function of assumed meteoroid mass and assumed KE-to-RF conversion efficiency (η)

Mass (g)	Velocity (Km/s) $\eta=0.0001\%$		Velocity (Km/s) $\eta=0.001\%$		Velocity (Km/s) $\eta=0.01\%$	
	PolA	PolB	PolA	PolB	PolA	PolB
1	375.6	273.2	118.7	86.4	37.5	27.3
10	118.7	86.4	37.5	27.3	11.8	8.64
30	68.5	49.88	21.6	15.7	6.8	4.9

Note that with resultant impossibly high meteoroid speeds, low mass events at low conversion efficiency are clearly ruled out. Possible impact speeds are less than ~ 70 km/s and, given the lack of atmosphere, greater than lunar escape speed which is ~ 2.2 km/s. As the observable lunar surface was exposed to the meteoroid apex (of Earth's way) source, the expected meteoroid speed is ≥ 30 km/s

Table 5 Time of the event, ALFA beam number, crest factor and Kinetic Energy estimates (assuming 0.001% efficiency and $m=10$ g) of the seven possible EMP events

Event number	1	2	3	4	5	6	7
Day of observation	2	1	1	1	1	1	1
Event Time offset from the start time on the day of observation (min)	24.36	16.15	44.36	46.55	66.1533	66.1583	124.012
ALFA Beam number	2	2	6	1	0	2	0
Time difference between the peaks in PolA and PolB (msec)	-0.19	0.75	0.7	-0.22	0.015	0.214	0.62
Crest factor Pol A (dB)	11.5	10.65	12.93	12.85	11.43	12.7	11.7
Crest factor Pol B (dB)	12.8	12.5	11.5	11.086	13.25	11.2	12.7
Kinetic Energy PolA (J)	1.35×10^7	7.5×10^6	7.05×10^6	6.25×10^6	9.03×10^6	5.8×10^6	1.8×10^7
Kinetic Energy Pol B (J)	7.5×10^4	4.08×10^6	3.73×10^6	3.89×10^6	1.2×10^7	3.5×10^6	8.8×10^6

Start time of observations on each day are given in Table 1. These events are shown in Figs. 13 and 14

The operating frequency for these observations was chosen in the IAU HI “protected band” (1370–1427 MHz) centered at 1410 MHz. Our preliminary results show that many of the transient EMP-like signals that were detected above the 3.5σ threshold (5 of the 7 “finalist” events were above 4σ) were due to a local out-of-band interfering radar observed as chirp signals of 1.5 MHz bandwidth generated as non-linear intermodulation artifacts in the receiver front-end low noise amplifier (LNA). These “events” were easily eliminated but at the cost of discarding much observational data. The separation of the remaining interference peaks from the possible on-source EMP events was accomplished via comparison of on-source versus off-source results from the various beams over the observing period and by masking-out the region of maximum interference. This resulted in identification (detection) of seven possible impact events at the event energy of $\sim 1.8 \times 10^7$ J (assuming KE-to-RF conversion efficiency of 0.001% and 10 g mass) in the ~ 5.5 h observing period. Assuming that, at any given time, four beams of the ALFA array system are on the

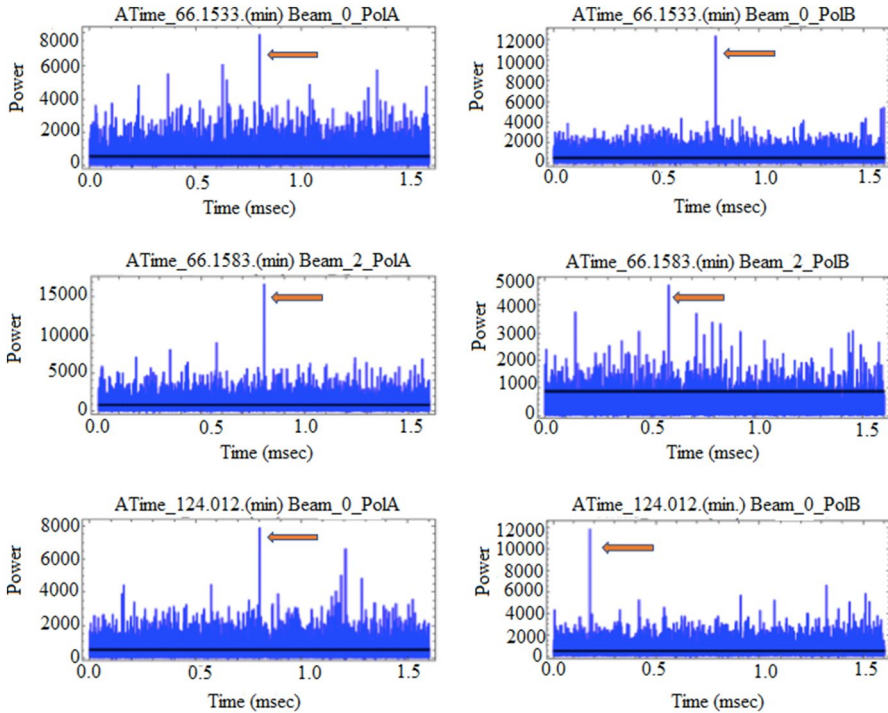


Fig. 14 Power versus time plots for *possible* Events 5–7 for both polarizations in their respective beams. The top event (Event 5) satisfies our hypothesis transient EMP definition with very small delay (for exact delay see Table 5). The black lines indicate the average power calculated from 100 ms time window

Moon and that each beam subtends ~ 11 arcminutes (assuming that the sidelobe response covers the entire area and that the entire 4-beam covered area is EMP-sensitive—the calculated power/energy from the observations is found using the lower sidelobe-sensitivity limit) at a distance of 365.8×10^6 km, gives the average observed lunar surface collecting area to be 4.21×10^6 km² ($\sim 11\%$ of the lunar surface area) thus yielding an impact event flux of $\sim 3 \times 10^{-7}$ (events) km⁻²h⁻¹ where the net observing time includes the reduction due to interference masking. This compares well with the event flux of the optical flashes reported in Suggs et al. (2014) who report an impact flux of $\sim 1.7 \times 10^{-7}$ (events) km⁻²h⁻¹. Our result is slightly larger than that derived from the visible flash observations for their limiting energy 1.3×10^7 J events. However, since the optical flux estimate values correspond to ~ 266 -hour observing period, we would need to observe for a much longer duration to achieve statistical significance in comparison with the optical results. Additionally, we note that the duration of the detected RF dual-polarization EMP events are of the order of few microseconds in a 1.6 ms window (Figs. 13, 14). This is consistent with our initial hypothesis based on the theory that the plasma is generated in the initial stage of the impact ejecta evolution followed by emission in visible domain. Note that we cannot at this point predict EMP polarization properties especially from near the limb given lunar surface features and dielectric properties, etc. However, if the events we report are indeed meteoroid-impact EMPs, then the evolution of the plasma generates the dual-polarization

EMPs at somewhat different times. This result, if confirmed, is important information on the RF-emission process, which is clearly much different than that of optical emissions.

Furthermore, the lunar noise temperature variations at the cold-hydrogen wavelength are reported. This seems to be an interesting result and we plan to explore it further. Finally, we find that for the ALFA system the HI protective band (1406–1412 MHz) is not fully “protected”. This is due to the strong-out-of-band PB radar that overloads the ALFA LNAs generating the significant in-band intermodulation interference. Power line arc impulses generated within the receiver system are also a possible source of some interference. Terrestrial Origin Moon Bounce (TOMB) signals were not observed at this frequency compared to the data collected at 440 MHz confirming that, as should be the case, no terrestrial radars or other transmitters operate in this protected frequency band and illuminate the Moon. In future, full validation of lunar impact EMPs at AO would appear to require parallel optical observations or independent observations from Haystack or GBT. Additionally, the ALFA array center frequency can be changed to 1412 MHz to mitigate the local chirp signal interference. Alternatively, the Long Wavelength Array, LOFAR, and other instruments can be utilized in an attempt to observe this phenomenon.

6 Conclusions

Detection of EMPs originating from meteoroid strikes on the Moon would inform many areas of science and engineering (e.g., Close et al. 2010, 2013). Conversely, if lunar impact EMPs are not detected, the physics would also be very interesting. With this in mind, we report the properties of seven *possible* such events observed using the Arecibo Observatory cold-hydrogen band ALFA system over ~5.5 h of observations. *IF* these are impact-generated EMPs, the event flux is roughly that reported for impact-generated optical flashes (Rembold and Ryan 2015; Suggs et al. 2014)—i.e., $\sim 3 \times 10^{-7}$ (events) $\text{km}^{-2} \text{h}^{-1}$. We find that these events correspond best to 10 gm and smaller meteoroids, given a kinetic energy to radio frequency conversion efficiency of 0.001%, rather than the kilogram-class meteoroids suggested by Suggs et al. As in our previous ~440 MHz observations (Kesaraju et al. 2016), impulsive interference has proven to be a substantial obstacle to unambiguous detection of EMPs. All else aside, we have established that future attempts to observe meteoroid-strike EMPs will require development of even more robust techniques to prevent, detect, and eliminate interference.

Acknowledgements This effort was supported under NSF Grants ATM 07-21613 and AGS 12-02019 to The Pennsylvania State University. The Arecibo Observatory was, at the time of these observations, operated by SRI International under a cooperative agreement with the National Science Foundation (AST-1100968), and in alliance with Ana G. Méndez-Universidad Metropolitana, and the Universities Space Research Association. We thank our reviewers, especially the final reviewer, for a most valuable contribution to this paper.

References

- Z. Ceplecha, J. Borovička, W.G. Elford, D.O. ReVelle, R.L. Hawkes, V. Porubčan et al., Meteor phenomena and bodies. *Space Sci. Rev.* **84**, 327–471 (1998)
- S. Close, M. Oppenheim, S. Hunt, A. Coster, A technique for calculating meteor plasma density and meteoroid mass from radar head echo scattering. *Icarus* **168**, 43–52 (2004)
- S. Close, P. Colestock, L. Cox, M. Kelley, N. Lee, Electromagnetic pulses generated by meteoroid impacts on spacecraft. *J. Geophys. Res. Space Phys.* **115** (2010)

- S. Close, I. Linscott, N. Lee, T. Johnson, D. Strauss, A. Goel, et al., Detection of electromagnetic pulses produced by hypervelocity micro particle impact plasmas. *Phys. Plasmas* (1994-present) **20**, 092102 (2013)
- A. Collette, K. Drake, A. Mocker, Z. Sternovsky, T. Munsat, M. Horanyi, Time-resolved temperature measurements in hypervelocity dust impact. *Planet. Space Sci.* **89**, 58–62 (2013)
- D. Ferguson, S. White, R. Rast, D. Thompson, D. Suszcynsky, K. Balasubramaniam, et al. A ground-based surveillance campaign to detect GPS arcing—first preliminary positive results, presented at the 14th Spacecraft Charging Technology Conference (2016)
- S. Ellingson, G. Hampson, Mitigation of radar interference in L-band radio astronomy. *Astrophys. J. Suppl. Ser.* **147**, 167 (2003)
- D.C. Ferguson, J. Murray-Krezan, D.A. Barton, J. Dennison, S.A. Gregory, Feasibility of detecting spacecraft charging and arcing by remote sensing. *J. Spacecr. Rockets* **51**, 1907–1913 (2014)
- D. Ferguson, S. White, R. Rast, K. Balasubramaniam, D. Thompson, D. Suszcynsky et al., Ground-based surveillance campaign to detect global positioning system arcing: first preliminary results. *J. Spacecr. Rockets* **54**, 566–571 (2017)
- L. Foschini, Electromagnetic interference from plasmas generated in meteoroids impacts. *EPL* **43**, 226 (1998)
- C. Heiles, Accurate parametric representation of ALFA main beams and first sidelobes, 1344–1444 MHz. http://www.astro.cornell.edu/~haynes/pre204/docs/heiles_beams.pdf (2004)
- C. Heiles, F. Drake, The polarization and intensity of thermal radiation from a planetary surface. *Icarus* **2**, 281–292 (1963)
- S. Kesaraju, J.D. Mathews, J. Vierinen, P. Perillat, D.D. Meisel, A search for meteoroid lunar impact generated electromagnetic pulses. *Earth Moon Planets* **119**, 1–21 (2016)
- K. Maki, T. Takano, A. Fujiwara, A. Yamori, Radio-wave emission due to hypervelocity impacts in relation to optical observation and projectile speed. *Adv. Space Res.* **34**, 1085–1089 (2004)
- K. Maki, E. Soma, T. Takano, A. Fujiwara, A. Yamori, Dependence of microwave emissions from hypervelocity impacts on the target material. *J. Appl. Phys.* **97**, 104911 (2005)
- J. Mathews, D. Janches, D. Meisel, Q.H. Zhou, The micrometeoroid mass flux into the upper atmosphere: arecibo results and a comparison with prior estimates. *Geophys. Res. Lett.* **28**, 1929–1932 (2001)
- D. Morabito, Lunar noise-temperature increase measurements at S-Band, X-Band, and Ka-band using a 34-meter-diameter beam-waveguide antenna. *Interplanet. Netw. Prog. Rep.* **42**, 166 (2006)
- I. Nemtchinov, V. Shuvalov, N. Artem'eva, B. Ivanov, I. Kosarev, I. Trubetskaya, Light flashes caused by meteoroid impacts on the lunar surface. *Sol. Syst. Res.* **32**, 99 (1998)
- L. Quintero, P. Perillat, RFI issues at the arecibo observatory, UPRM RFSMW (Radio Frequency Spectrum Management Workshop) (2016)
- P.R. Ratcliff, M.J. Burchell, M.J. Cole, T.W. Murphy, F. Alladfadi, Experimental measurements of hypervelocity impact plasma yield and energetics. *Int. J. Impact Eng.* **20**, 663–674 (1997)
- J.J. Rembold, E.V. Ryan, Characterization and analysis of near-earth objects via lunar impact observations. *Planet. Space Sci.* **117**, 119–126 (2015)
- R.M. Suggs, W.J. Cooke, R.J. Suggs, W.R. Swift, N. Hollon, The NASA lunar impact monitoring program. *Earth Moon Planet* **102**, 293–298 (2008)
- R. Suggs, D. Moser, W. Cooke, R. Suggs, The flux of kilogram-sized meteoroids from lunar impact monitoring. *Icarus* **238**, 23–36 (2014)
- T.L. White, J.R. Cogdell, Lunar polarization studies at 3.1 mm wavelength. *The Moon* **6**, 235–249 (1973)